This is a preprint, the final version is subject to change, of the American Mineralogist (MSA)
Cite as Authors (Year) Title. American Mineralogist, in press.
(DOI will not work until issue is live.) DOI: http://dx.doi.org/10.2138/am-2016-5379

Revision 2

Understanding magmatic processes at Telica volcano, Nicaragua: Crystal size distribution and textural analysis

Molly Witter[1,2]*, Tanya Furman[1], Peter LaFemina[1], Maureen Feineman[1]

[1] Department of Geosciences, Pennsylvania State University, University Park, PA 16802, USA

[2] Now at: Department of Geological Sciences, Stanford University, 397 Panama Mall, Stanford CA, 94305 USA

* Corresponding author: mrwitter@stanford.edu

Abstract

Telica volcano in Nicaragua currently exhibits persistent activity with continuous seismicity and degassing, yet it has not produced lava flows since 1529. To provide insight into magma chamber processes including replenishment and crystallization, crystal size distribution (CSD) profiles of plagioclase feldspar phenocrysts were determined for Quaternary Telica basalts and basaltic andesites. Textural analysis of fourteen highly crystalline lavas (>30 vol.% phenocrysts) indicates that the samples are dominated by sieve-textured plagioclase feldspar phenocrysts whose origin requires thermochemical disequilibrium within the magmatic system. The CSD curves display an inverse relationship between phenocryst length and population density. Concave-up patterns observed for the Telica lava samples can be represented by linear segments that define two crystal populations: a steeply-sloping segment for small crystals (<1.5 mm) and a gently-sloping segment for crystals >1.5 mm in length. The two crystal populations may be explained by magma replenishment and a mixing model in which a mafic magma is introduced to a stable chamber that is petrologically and geochemically evolving. Residence times calculated using the defined linear segments of the CSD curves suggest these magmatic processes occur over time scales on the order of decades to centuries. The crystal size distribution and textural analysis advocate for the current persistent activity as being consistent throughout Telica's historic and prehistoric eruptive periods and driven by replenishment of mafic magma.

Keywords: Crystal size distribution, magma mixing, persistent volcanoes, sieve texture, disequilibrium, Telica volcano, plagioclase feldspar

Introduction

Magmatic processes are commonly investigated through sampling of volcanic rocks and the application of quantitative geochemical elemental and isotopic analysis. The preservation of the crystallization history in igneous rocks also allows for quantitative textural analyses to be performed. The crystal size distribution (CSD) method, developed by Randolph and Larson (1971) for chemical engineering purposes and introduced to the geologic field by Marsh (1988) and Cashman and Marsh (1988), is useful for investigating ancient and historic magmatic processes. Measuring the CSD profiles of rock samples provides insight into magmatic processes including fractional crystallization, magma injection and mixing, and crystal nucleation and growth, as well as allowing estimates of residence times (Marsh, 1988; 1998). This information may also potentially be used to infer future eruptive behavior of the volcanoes studied.

Telica volcano, located in north-western Nicaragua (Fig. 1a), is one of the most active volcanoes of the region, yet the magmatic processes causing this activity are not well constrained for this system. It is referred to as a persistently active volcano (Locke et al., 2003) because it displays nearly continuous seismic activity and degassing. The TElica Seismic ANd Deformation (TESAND) network was installed in 2010 to monitor this persistent activity in hopes of better understanding eruption precursors such as those associated with the May 2011 eruption (Geirsson et al., 2014). Though the last recorded lava flow at Telica was in 1529, incandescence has been observed periodically during the past two decades (Smithsonian Institution Global Volcanism Program) and the persistent activity is punctuated by periods of phreatic vulcanian explosive activity, up to VEI 2. The most recent eruptive phase occurred in 2011 (Geirsson et al., 2014). Increased monitoring instrumentation at Telica has improved the understanding of the persistent activity (Rodgers et al. 2015), but much remains in question regarding prior and current magmatic processes.

Textural distributions of plagioclase feldspar crystals from historic and prehistoric basalt and basaltic andesite flows from Telica volcano provide new evidence to better constrain the magmatic kinetics of this unusual system. Observed textural patterns and CSD curves from Quaternary lava flows, interpreted in light of the bulk lava chemistry, indicate pervasive thermochemical disequilibrium within the magmatic system. These features are consistent with the mixing of magmas of distinct thermal and geochemical character, therefore creating thermochemical disequilibrium (Higgins and Roberge, 2007; Salisbury et al., 2008). This mixing may be the consequence of frequent influx of a predominantly mafic magma that is injected into the chamber, catalyzing or extending the eruptive period. Frequent temporary sealing of the eruptive conduit (Geirsson et al., 2014) that allows pressure to build up prior to eruption may be followed by rapid decompression that could also contribute to the formation of sieve-textured plagioclase (Nelson and Montana, 1992). These results support current models based on degassing emissions and seismic data that infer frequent (annual to decadal) and temporary sealing within the magma plumbing system (Geirsson et al., 2014), and suggest that the modern eruptive behavior of Telica has been persistent throughout its history.

Methods

Samples from 14 representative Quaternary Telica lava flows (Carr et al., 2007) were collected at varying distances from the currently active crater in May 2011 by Witter (Fig. 1). Unaltered, minimally weathered lava flow outcrops were targeted for collection. Rock samples were prepared for textural and geochemical analysis at The Pennsylvania State University. Samples were cut into slabs with weathered portions removed, polished and reduced to ~5-7 mm pieces using an alumina ceramic mini-crusher. Powders were prepared by grinding in a tungsten carbide shatter box for 30-90 seconds. Whole-rock analyses for major and minor elements (including Ba and Sr) were obtained by Directly Coupled Plasma (DCP) spectroscopy on an ARL-Fisons Spectraspan 7; remaining trace elements were analyzed by Inductively Coupled Plasma Mass Spectrometry (ICP-MS) using a VG PlasmaQuad-3. Precision reproducibility based on replicate analyses of samples and natural basalt standards is generally <1% for SiO_2, Sr, Y, Zr, Nb, La, Ce; <3% for other major elements, Ba, Sr, Rb, Cs, Cr, Sc, V, Co, Pr, Nd, Sm, Eu, Gd, Tb, Dy, Ho, Er, Hf and Ta; <5% Ni, Yb, Lu, Pb, Th and <8% for U (Table 1).

Standard thin sections (30μm thickness) were prepared from representative billets cut from the 14 samples and optical microscopy was carried out on all thin sections to document plagioclase feldspar phenocryst abundances, shapes and textures. Images of the thin sections for quantitative textural analysis (Fig. 2) were obtained using a microfiche black and white scanner. Electron microprobe analysis of individual plagioclase feldspar phenocrysts was carried out on the most mafic (MT11-12) and most evolved (MT11-7) samples collected. Analysis was completed at Stanford University using a JEOL JXA-8230 electron microprobe under operating conditions of 20 nA, an accelerating voltage of 15 keV, and beam size of 2 μm in diameter.

Image processing using ImageJ 1.46 software was performed to obtain size measurements of the plagioclase phenocrysts. Long and short axes of the plagioclase crystals were measured and counted (100 per thin section) to calculate the aspect ratio of each crystal. The CSDslice template (Morgan and Jerram, 2006) and database were used to estimate 3-dimensional crystal habits from the 2-dimensional measurements. Assuming that all the crystals in the 2-dimensional thin section have the same habit, the ratio of the short, intermediate, and long-axis (referred to as the shape factor, e.g., Innocenti et al. 2013) can be determined using best-fit estimates. This aspect ratio, determined to be 1.0**:**3.4**:**4.0 for Telica lavas, was used in CSD Corrections V.1.4.0.2 (Higgins, 2000; 2002a) to create the CSD curves. CSD Corrections addresses the dependence of crystal population density on the distribution and orientation of the phenocrysts. Roundness was estimated to be 0.1 based on visual observations (0 = block, 1 = ellipsoid). Long axes only of all plagioclase phenocrysts per given area were measured (300 to 515 per thin section) to give a representative size distribution of the samples (Morgan and Jerram, 2006; Innocenti et al., 2013). The CSDs reported in this study do not have vesicle content corrections because the samples have low vesicularity (<5 vol.%).

Results

Major and trace element geochemistry

Bulk analyses of Telica lavas sampled for this study range from 48.48 to 54.19 wt.% SiO_2 (all iron as Fe^{+3}; Table 1). Samples are classified as basalts to basaltic andesites (Fig. 3), and plot within the range of basaltic and andesitic lava and bomb samples collected previously at Telica; all Telica analyses fall within the range observed along the Central American volcanic arc (Carr and Rose, 1987; Patino et al., 2000). The visible freshness of the lavas chosen for this study is confirmed by low loss on ignition (LOI) values that range from -0.4 to 1.2 wt.%. The high LOI value and noticeably lower SiO_2 content of sample MT11-RB may indicate minor alteration. MT11-12 is the most mafic sample collected during this study (6.14 wt.% MgO); MT11-7 is the most felsic sample (4.03 wt.% MgO).

The most mafic Telica lavas have smooth chondrite-normalized rare earth element (REE) profiles with a small negative Ce anomaly, weak downwards concavity in the middle REEs, and flattening in the heavy REEs (Fig. 4a). More evolved samples show greater development of a negative Ce anomaly, as well as negative Eu anomalies presumably resulting from removal of plagioclase feldspar. We suggest that, following Neal and Taylor (1989) the negative Ce anomaly reflects minor contributions from seawater-altered basalt and/or hemipelagic sediments. As the hemipelagic sediment input increases, Ba/Th decreases and U/La increases (Figure 5). Younger Telica lavas have a larger hemipelagic sediment component than older lavas (Carr et al., 2007). Abundances of incompatible trace elements, normalized to values for the primitive mantle (Sun and McDonough, 1989), show the saw tooth pattern typical of Telica lavas (Carr and Rose, 1987) with marked depletions in Nb, and Ta for all samples, Ti depletion for the evolved samples, and enrichments in Ba, U, K, Pb and Sr in the mafic samples (Fig. 4b). This signature has been interpreted as reflecting a mantle source domain dominated by depleted mantle with contributions from recycled sediments and slab-derived fluids (Carr et al., 2007).

Petrography

The lavas studied here are highly crystalline (>30% phenocrysts by volume). The most common phenocryst phase is plagioclase feldspar (~75 vol. %), followed by clinopyroxene (~10 vol. %)

with trace amounts of olivine (<5 vol. %) (Appendix A). Plagioclase feldspar phenocrysts are typically lath-shaped rectangular prisms. The plagioclase phenocrysts range in size from <100 μm to >3 mm and crystals of all sizes exhibit sieve textures or concentric zoning and clear homogeneous rims. The sieve textures are of variable appearance: some phenocrysts are heavily sieved from core to rim, while others exhibit zones of resorption (Fig. 2). Clinopyroxene phenocrysts are euhedral to rounded and commonly form glomerocrysts. Simple twinning of clinopyroxene is common and phenocrsyts range up to ~2 mm in size. Small equant olivine phenocrysts (0.05-0.2 mm) were present in most samples. All phenocrysts are set in a fine-grained plagioclase and Fe-Ti oxide matrix, and five of the fourteen samples have local patches of devitrified glass. Complete thin section descriptions can be found in the Appendix.

Morphometrical Data

The crystal size distribution (CSD) curves, resulting from the measurements of the long axes of individual plagioclase feldspar crystals in all 14 Telica lavas, are compiled in Figure 6. Here, the natural logarithm of the crystal population density is plotted versus the crystal length. Size bins that have fewer than 3 crystals are not included in the calculation of the CSD curves. Imaging resolution issues often occur within the smallest size fractions (<0.25 mm) where phenocryst identification becomes difficult. Because of this discrepancy, there may be a loss of validity of interpreting crystallization processes such as syn-ascent crystallization as recorded by very small size fraction crystals.

The crystal population densities for all the samples range from -8.4 to 3.8 (logarithmic scale) and are inversely correlated with the crystal length (i.e., the trends indicate smaller populations of larger crystals) (Fig. 6). The CSD pattern distributions are not linear; there is a clear trend of upward concavity in the CSD curves for all of the Telica lava samples. This pattern has been observed with other volcanic rocks and precludes the application of a single crystal population model (Marsh, 1988; Armienti, et al., 1994, Higgins and Roberge, 2007). Population density is relatively consistent for all samples for size fractions less than 1 mm, and greater variation between samples arises at larger size fractions (>1.5 mm). Seven of the samples (MT11-2, MT11-5, MT11-7, MT11-8, MT11-9, MT11-10 and MT11-12) have plagioclase crystals greater than 2 mm in length. The population densities for these larger size fractions are much more variable than those in the smaller size fraction bins, as illustrated by the fanning pattern (Fig. 6). Table 2 summarizes parameters used to calculate the CSDs and gives the slopes and intercepts of the different plagioclase populations, S1 and S2, for each sample. The differences in the slopes of the two populations (denoted as Δ Slope in Table 2) illustrates the degree of upward concavity of the samples, with lower numbers representing more linear CSD curves and higher numbers representing increased concavity.

Phenocryst Chemistry

Representative plagioclase feldspar analyses (Table 3) include both small crystals (S1, <1.5 mm) and larger phenocrysts (S2, >1.5 mm) from a more mafic sample, MT11-12, and a more evolved sample, MT11-7. All phenocrysts analyzed are normally zoned and exhibit sieve textures to varying degrees. Heavily sieved cores tend to have lower anorthite contents than cores that do not display sieve textures (e.g., compare plagioclase 4 and 5 in MT11-12 in Fig. 7). The S2 phenocrysts have similar core compositions in both samples despite differences in lava MgO content. In contrast, the S1 populations (small crystals) of these samples do not overlap. The more mafic sample has S1 core and rim compositions that are less anorthitic than those of the S1 phenocrysts in evolved lava MT11-7. In the magnesian sample MT11-12, core compositions of the plagioclase feldspars vary from An_{71-90} (average An_{79}), with rims of An_{57-72} (average An_{62}). The smaller crystals (S1) of MT11-12 have core and rim compositions that span a much narrower range and are generally not as An-rich as those of the larger (S2) crystals (Fig. 8). Interestingly, plagioclase feldspars in evolved lava MT11-7 have cores that extend to higher anorthite contents (An_{81-93}; average An_{87}) with highly variable rim compositions (An_{61-90}; average An_{72}). In this sample, the anorthite contents for S1 and S2 overlap to large extent, with the cores of S1 being weakly and unexpectedly more anorthitic.

Discussion

Interpretation of Telica CSD patterns

Crystal size distribution (CSD) theory and its applications (Marsh, 1988; Cashman and Marsh, 1988) provide a means to use plagioclase feldspar crystal abundances and size profiles to infer geological and magmatic processes. Most relevant to this work, plotting the natural logarithm of the crystal population density versus the crystal length (Fig. 6) gives an inversely proportional relationship that can be used to interpret crystallization histories. All Telica samples display curved or curvilinear CSD profiles (Fig. 6). This pattern of steeply-sloping CSD for small crystals and gently sloping CSD for larger crystals is interpreted broadly as evidence for reservoir replenishment at open-system volcanoes (Higgins, 1996; Innocenti et al., 2013). Replenishment events can cause mixing of magmas, convection and reheating in the chamber and conduit as well as addition of volatiles, melt and nucleation sites to the evolving system, potentially triggering an eruption (Sparks et al., 1977; Kent et al., 2010). Extreme slope changes within CSDs, referred to as "kinks", strongly indicate separate nucleation events (Burkhart et al., 1980; Marsh, 1998; Ngonge et al., 2013). A new magma input can allow for textural coarsening in the chamber or conduit and can establish crystal growth at different reservoir depths (Higgins and Roberge, 2003). Mixing and late-stage degassing may also induce nucleation events (Cashman and Marsh, 1988; Armienti et al., 1994; Higgins, 1996; Marsh, 1998). Telica CSDs illustrate sharply curved patterns that can be represented by two line segments of distinct slope, indicating an open-system magmatic reservoir (Mock et al., 2003; Mock and Jerram, 2005; Berger et al., 2008). We note in addition that the pervasive occurrence of sieve textures in plagioclase feldspars of all sizes, as well as the wide range and distribution of feldspar compositions, point strongly towards a model of open-system behavior with frequent replenishment by mafic magma inputs.

We recognize that several other mechanisms may contribute to generation of curved or kinked CSD patterns. Marsh (1988) noted that concave-upwards CSDs could result from the accumulation of large plagioclase crystals within a magma body. Though plagioclase feldspar is the dominant phenocryst in all samples, there is no compelling evidence for this interpretation of the Telica samples. Note that the REE profiles (Fig. 4) of mafic (MT11-12 and MT11-2), intermediate (MT11-8 and MT11-RB) and felsic (MT11-6 and MT11-7) Telica samples (normalized to chondritic values of Sun and McDonough, 1989) all lack positive europium anomalies that would be expected with plagioclase accumulation.

Curved CSDs may also result if the growth rate of the crystals is dependent on their size, or if small crystals are resorbed during the growth of neighboring larger crystals (fines destruction or textural coarsening; Marsh, 1988; DeHoff, 1991). The "Communicating Neighbors" model (DeHoff, 1991) notes that if a large crystal is surrounded by other large crystals during textural coarsening, solution of grains will not occur and the large crystals will not have the necessary nutrients for growth. This process would lead to variability in growth history between phenocrysts, but it is unclear whether textural coarsening can be applied to volcanic rocks as it has been for plutonic rocks (Hunter, 1987, 1996; Higgins, 1998, 2002b). Rapid changes in magma cooling rates may produce curved CSD plots if slow cooling occurs at depth and rapid cooling occurs higher in the conduit (Maaloe et al., 1989). This mechanism will produce two different crystal size populations as the nucleation rate of the magma varies. However, the change in the nucleation rate is expected to be recorded in the CSD as a step, followed by a return to the same slope, (Higgins, 1996) rather than the concave-up pattern observed at Telica. Taken together, all lines of argument support pervasive open-system behavior of magmatic processes at Telica and indicate that the CSD patterns may provide insight into the time scales of these important processes and phenomena.

CSD studies have been employed at other persistently active volcanoes, such as Stromboli (Armienti et al., 2007). The concave-up CSD patterns observed at Telica are not observed for the eruptions at Stromboli between 1984 and 2003. Stromboli lavas produce linear CSD patterns for crystals 0.06-1.2 mm. The uniformity of the slopes and intercepts of the plagioclase at Stromboli indicate that the conditions under which the plagioclase CSDs formed were unvarying over the study period, and the CSD patterns are interpreted as indicating a system at equilibrium, with frequent replenishment by basaltic magma (Armienti et al., 2007). Table 2 shows the slopes and intercepts for the Telica CSDs. For the smaller plagioclase population (< 1.5 mm), there is little variation of the slopes and intercepts, similar to what is observed at Stromboli (Armienti et al., 2007). MT11-1 and MT11-RB have steeper slopes for the larger plagioclase population, S2, but the majority of the samples have a slopes that span a narrow range. As suggested by Armienti et al. (2007), the constant intercepts and slopes suggest repetition over time of the processes that form these different plagioclase populations.

The Telica lavas do not show consistent correlations between plagioclase feldspar size distribution with silica or MgO content, indicating that the CSD patterns are not necessarily dictated by the major element geochemistry. MT11-RB, the most silica-poor sample but with intermediate MgO content (48.48 wt.% SiO_2, 4.51 wt.% MgO), has the most linear CSD curve (Fig. 6 dotted line). MT11-12, with intermediate silica content and the highest MgO content (51.18 wt.% SiO_2, 6.18 wt.% MgO), has the CSD pattern displaying the greatest upward concavity and largest crystal size range (Fig. 6 dashed line). Direct comparison between these two samples may be problematic given the limit of larger size fractions in MT11-RB. However, it is valuable to note that the most primitive sample (MT11-12) and the most evolved sample (MT11-7) in this study have similar slope transitions, indicating that the population densities are similar and MgO content does not control the CSD patterns.

Residence Times

The upward concavity of the CSD curves can be represented effectively by two distinct linear segments that describe the distribution of crystal sizes (Fig. 6). The more steeply sloping line represents the smaller crystal population, S1, while the more shallowly sloping line represents the larger crystals, S2. Residence times of the populations can be calculated using the equation:

$$slope = \frac{-1}{\text{growth rate} \times \text{residence time}}$$ (Higgins, 1996).

The intercept of the line represents the nucleation density. Under the assumption that the growth rate is constant with crystal size (Cashman and Marsh, 1988) and at a rate of 10^{-10} mm/s (Cashman, 1988), geologically reasonable residence times of the Telica crystal population are calculated and summarized in Table 2. This growth rate was chosen based on work on systems of similar chemical composition (Cashman, 1993).

The residence time for the small crystals is estimated to be ~63 years, while larger crystals have a residence time of ~171 years. Calculations of residence times at several basaltic volcanoes by Gauthier et al. (2000) and Pietruszka and Garcia (1999) show typical ranges of tens to hundreds of years, as suggested for Telica. Because the calculation of the residence times is heavily dependent on the separation of the data into two lines with distinctly different slopes, the calculated residence times are better used as a qualitative guide rather than a precise indicator of crystal storage time.

Magmatic Processes at Telica

Petrographic and microprobe analysis results show that the vast majority of Telica plagioclase feldspar phenocrysts, regardless of size, display sieve textures and complex compositional zoning (Figs. 2, 6). Sieve textures are emblematic of thermochemical disequilibrium in the magmatic system. Magma mixing and rapid decompression associated with ascent have been invoked to explain the production of sieve-textured plagioclase (Dungan and Rhodes, 1978; Tsuchiyama, 1985; Nelson and Montana, 1992). Recent explosions at Telica are relatively low intensity (up to VEI 2), demonstrating a lack of large pressure buildup between eruptions

(Geirsson et al., 2014). If the current persistent activity is representative of Telica's history, the low intensity explosions and lack of edifice deformation that could be associated with magma ascent indicate that the sieve texture is mostly likely not a result of ascent-related rapid decompression. Rather, the textural and chemical features, including An-rich cores in feldspars within evolved Telica lavas, support a significant role for magma mixing processes at Telica (Neave et al., 2013).

The anorthitic plagioclase in both mafic and felsic samples suggest that additional plagioclase come from a mafic magma, implying a basaltic input to the chamber. The similar compositions of the S2 populations, regardless of bulk rock chemistry, indicate that a mafic magma distributes the large An-rich crystals throughout the system. The S1 population in the mafic lavas reflect the composition of the melt; showing lower anorthite contents as the mafic input mixes with the slightly evolved system. Melt compositions are also represented in the S1 population of the felsic lavas. The S1 high anorthite contents in the felsic lavas can be produced by mixing of a crystal-poor evolved magma in the chamber with a plagioclase-rich mafic input. Because the replenishing mafic magma is less viscous than the evolved chamber magmas, the S1 population can easily nucleate from the mafic replenishment. The formation of an S1 population in the felsic magma in the chamber is hindered by the higher viscosity and slower diffusion.

The persistent activity recorded at Telica since the first seismometer was installed in 1993 is characterized by nearly constant seismic activity (Rodgers et al., 2011) and degassing. In order for volcanoes to maintain persistent degassing, there must be a supply of gas-rich magma, which needs to be accommodated at some depth beneath the volcanic edifice (Francis et al., 1993;

Locke et al., 2003). Recent eruptions at Telica, such as that of May 2011, have produced little juvenile material (Witter et al., 2011; Geirsson et al., 2014), but incandescence has been observed in the months following the eruptive activity, similar to the 1999 activity. Seismicity is centered under the active crater, suggesting that dike propagation is not the major pathway for magma accommodation (Rodgers et al., 2015). Microgravity studies at Telica from 1994-2000 find consistent net gravity changes throughout the entire survey area of the edifice. This observation differs from those made at other persistently active volcanoes in Central America, such as Poas, Costa Rica (Locke et al., 2003) and suggests that mass distribution is not localized beneath the active crater, but rather that small mass increases of magma occur over the total survey area of the volcanic edifice at shallow depths over the course of several years. Shallow microgravity variations also occur over shorter time periods (on the scale of minutes to hours), but are typically more complex, spatially limited, and associated with Strombolian eruptions. Taken together, the microgravity and seismic observations support a model based on inferences from petrography, mineral chemistry and CSD observations in which a magma in a spatially expansive and complex plumbing system that is undergoing fractional crystallization is interrupted by frequent replenishment of new batches of magma.

Implications

This study highlights the textures of plagioclase-dominated basalt and basaltic andesite Telica lavas with prominent sieve textures. Crystal size distribution profiles of these lavas record the presence of two different feldspar populations, indicating distinct crystallization histories that require open-system magmatic behavior. Curved CSD patterns, sieve-textured plagioclase phenocrysts, and glassy zones in the groundmass could suggest repeated interaction between a

This is a preprint, the final version is subject to change, of the American Mineralogist (MSA)
Cite as Authors (Year) Title. American Mineralogist, in press.
(DOI will not work until issue is live.) DOI: http://dx.doi.org/10.2138/am-2016-5379

stable, degassed shallow magma body with a mafic input. Zoning patterns and core compositions of plagioclase feldspars in all size ranges give strong support to this interpretation. Small mass increases, as suggested by microgravity studies, may occur at a greater depth than the degassing magma body, causing the two bodies to develop distinct geochemical or petrographic signatures. The mixing of these thermochemically-distinct magma batches creates lavas with two different sized plagioclase feldspar populations, both with complex zoning patterns and abundant sieve textures. These mixing events provide a possible eruptive trigger related to devolatization of the replenishing mafic magma.

Calculation of approximate residence times indicates that magmatic processes operating on the order of centuries are recorded by the larger crystals, while decade-scale processes are reflected in the smaller crystal population. These distinctly different size populations may arise from magmatic processes occurring at different depths, consistent with complex microgravity readings observed at Telica. Persistent restless behavior at Telica appears to be a consistent feature of its evolution, and likely reflects the interplay between frequent replenishment at depth and periodic sealing and opening of the shallow level conduit(s). The application of quantitative textural and geochemical analysis on persistently active volcanoes coupled with current seismic, deformation and degassing monitoring can elucidate complex magmatic processes, such as those at Telica.

Acknowledgements

Fieldwork in Nicaragua was supported by NSF EAR 0911366 awarded to LaFemina and completed with assistance from Halldor Geirsson and Mel Rodgers. Analytical support came from the WISER program (NASA PA Space Grant) at The Pennsylvania State University. Whole rock analysis was completed by Gary Dwyer at Duke University. Furman gratefully acknowledges support from NSF DUE 0962792.

References Cited

Armienti, P., Pareschi, M.T., Innocenti, F. & Pompilio, M. (1994) Effects of magma storage and ascent on the kinetics of crystal-growth - the case of the 1991-93 Mt. Etna eruption. Contributions to Mineralogy and Petrology 115, 402-414.

Armienti, P., Francalanci, L., & Landi, P., (2007) Textural effects of steady state behaviour of the Stromboli feeding system. Journal of Volcanology and Geothermal Research 160, 86-98.

Berger, J., Ennih, N., Liégois, J.-P., Nkono, C., Mercier, J.-C.C. & Demaiffe, D. (2008) A complex multi-chamber magmatic system beneath a late Cenozoic volcanic field: evidence from CSDs and thermobarometry of clinopyroxene from a single nephelinite flow (Djbel Saghro, Morocco). Geological Society of London, Special Publication 297, 509–524.

Burkhart, L.E., Hoyt, R.C. & Oolman, T. (1980) Control of particle size distribution and agglomeration in continuous precipitations. In: Kuczynski, G.C. (Ed.), Sintering Processes. Plenum, NY, pp. 23–38.

Carr, M.J. & Rose, W.I. (1987) CENTAM – a data base of analyses of Central American volcanic rocks. Journal of Volcanology and Geothermal Research 33. (http://www-rci.rutgers.edu/ ~carr/index.html)

Carr, M.J., Saginor, I., Alvarado, G.E., Bolge, L.L., Lindsay, F.N., Milidakis, K., Turrin, B.D., Feigenson, M.D. & Swisher III, C.C. (2007) Element fluxes from the volcanic front of Nicaragua and Costa Rica. Geochemistry, Geophysics, Geosystems 8, Q06001.

Cashman, K.V. (1988) Crystallization of Mount St. Helens 1980-1986 dacite: a quantitative textural approach. Bulletin of Volcanology 50, 194-209.

Cashman, K.V. & Marsh, B.D. (1988) Crystal Size Distribution (CSD) in rocks and the kinetics and dynamics of crystallization II: Makaopuhi lava lake. Contributions to Mineralogy and Petrology 99, 292-305.

Cashman, K.V. (1993) Relationship between plagioclase crystallization and cooling rate in basaltic melts. Contributions to Mineralogy and Petrology 113, 126–142.

Dehoff, R.T. (1991) A geometrically general-theory of diffusion controlled coarsening. Acta Metallurgica Et Materialia 39, 2349-2360.

Dungan, M.A. & Rhodes, J.M. (1978) Residual glasses and melt inclusions in basalts from DSDP LEGS 45 and 46—evidence for magma mixing. Contributions to Mineralogy and Petrology 67, 417-431.

Francis, P., Oppenheimer, C. & Stevenson, D. (1993) Endogenous growth of persistently active volcanoes. Nature 366, 554-557.

Gauthier, P.J., Le Cloarec, M.F. & Condmines, M. (2000) Degassing processes at Stromboli Volcano inferred from short- lived disequilibria (^{210}Pb-^{210}Bi-^{210}Po) in volcanic gases. Journal of Volcanology and Geothermal Research 102, 1-19.

Geirsson, H., Rodgers, M., LaFemina, P., Witter, M., Roman, D., Muñoz, A., Tenorio, V., Alvarez, J., Jacobo, V. C., Nilsson, D., Galle, B., Feineman, M. D., Furman, T. & Morales, A. (2014) Multidisciplinary observations of the 2011 explosive eruption of Telica volcano, Nicaragua: implications for the dynamics of low-explosivity ash eruptions. Journal of Volcanology and Geothermal Research 271, 55-69.

Higgins, M.D. (1998) Origin of anorthosite by textural coarsening: quantitative measurements of a natural sequence of textural development. Journal of Petrology 39, 1307–1325.

Higgins, M.D. (2000) Measurement of crystal size distributions. American Mineralogist, 85, 1105–1116.

Higgins, M.D. (2002a) Closure in crystal size distributions (CSD), verification of CSD calculations, and the significance of CSD fans. American Mineralogist 87, 913-931.

Higgins, M.D. (2002b) A crystal size-distribution study of the Kiglapait layered mafic intrusion, Labrador, Canada: evidence for textural coarsening. Contributions to Mineralogy and Petrology 144, 314–330.

Higgins, M.D. & Roberge, J. (2003) Crystal size distribution (CSD) of plagioclase and amphibole from Soufriere Hills volcano, Montserrat: evidence for dynamic crystallization/textural coarsening cycles. Journal of Petrology 44, 1401–1411.

Higgins, M.D. & Roberge, J. (2007) Three magmatic components in the 1973 eruption of Eldfell volcano, Iceland: Evidence from plagioclase crystal size distribution (CSD) and geochemistry. Journal of Volcanology and Geothermal Research 161, 247–260.

Hunter, R.H. (1987) Textural equilibrium in layered igneous rocks. In: Parsons, I. (Ed.), Origins of Igneous Layering. D Reidel, 473–503.

Hunter, R.H. (1996) Textural development in cumulate rocks. In: Cawthorn, R.G. (Ed.), Layered Intrusions. Developments in Petrology, 77–101.

Innocenti, S., Furman, T., Voight, B. & Andreastuti, S. (2013) Textural and mineral chemistry constraints on evolution of Merapi Volcano, Indonesia. Journal of Volcanology and Geothermal Research 261, 20-37.

Kent, A.J.R., Darr, C., Koleszar, A.M. & Salisbury, M.J. (2010) Preferential eruption of andesitic magmas through recharge filtering, Nature Geoscience 3, 631-636.

Locke, C.A., Rymer, H. & Cassidy, J. (2003) Magma transfer processes at persistently active volcanoes: insights from gravity observations. Journal of Volcanology and Geothermal Research 127, 73-86.

Maaloe, S., Tumyr, O. & James, D. (1989) Population-density and zoning of olivine phenocrysts in tholeiites from Kauai, Hawaii. Contributions to Mineralogy and Petrology 101, 176-186.

Marsh, B.D. (1988) Crystal Size Distribution (CSD) in Rocks and the Kinetics and Dynamics of Crystallization.1. Theory. Contributions to Mineralogy and Petrology 99, 277-291.

Marsh, B. D. (1998) On the interpretation of crystal size distributions in magmatic systems. Journal of Petrology 39, 533-600.

Mock, A., Jerram, D.A. & Breitkreuz, C. (2003) Using quantitative textural analysis to understand the emplacement of shallow level rhyolitic laccoliths: a case study from the Halle volcanic complex, Germany. Journal of Petrology 44, 833–849.

Mock, A. & Jerram, D.A. (2005) Crystal size distributions (CSD) in three dimensions: in- sights from the 3D reconstruction of a highly porphyritic rhyolite. Journal of Petrology 46, 1525–1541.

Morgan, D.J. & Jerram, D.A. (2006) On estimating crystal shape for crystal size distribution analysis. Journal of Volcanology and Geothermal Research 154, 1-7.

Neal, C.R. & Taylor, L.A. (1989) A negative Ce anomaly in a peridotite xenolith: Evidence for crustal recycling into the mantle or mantle metasomatism?. Geochemica et Cosmochimica Acta 53, 1035-1040.

Neave, D.A., Passmore, E., Maclennan, J., Fitton, G., & Thordarson, T. (2013) Crystal-melt relationships and the record of deep mixing and crystallization in the AD 1783 Laki eruption, Iceland. Journal of Petrology 54, 1661-1690.

Nelson, S.T. & Montana A. (1992) Sieve-textured plagioclase in volcanic rocks produced by rapid decompression. American Mineralogist 77, 1242-1249.

Ngonge, D.E., Archanjo, C.J. & Hollanda, M.H.B.M. (2013) Plagioclase crystal size distribution in some tholeiitic mafic dykes in Cabo Frio-Buzios, Rio de Janeiro, Brazil. Journal of Volcanology and Geothermal Research 255, 26-42.

Patino, L.C., Carr, M.J. & Feigenson, M.D. (2000) Local and regional variations in Central American arc lavas controlled by variations in subducted sediment input. Contributions to Mineralogy and Petrology 138, 265-283.

Pietruszka, A.J. & Garcia, M.O. (1999) The size and shape of Kilauea Volcano's summit magma storage reservoir: a geo- chemical probe. Earth and Planetary Science Letters 167, 311-320.

Randolph A.D. & Larson M.A. (1971) Theory of particulate processes. Academic Press, New York.

Rodgers, M., Roman, D.C., Geirsson, H., La Femina, P.C., Witter, M.R., Muñoz, A. & Tenorio, V. (2011) Seismicity associated with the May 2011 eruption of Telica Volcano, Nicaragua, Abstract V53E-2671 presented at 2011 Fall Meeting, AGU, San Francisco, Calif., 5-9 Dec.

Rodgers, M., Roman, D. C., Geirsson, H., LaFemina, P., McNutt, S. R., Muñoz, A., & Tenorio, V. (2015). Stable and unstable phases of elevated seismic activity at the persistently restless Telica Volcano, Nicaragua. Journal of Volcanology and Geothermal Research 290, 63-74.

Salisbury, M.J., Bohrson, W.A., Clynne, M.A., Ramos, F.C. & Hoskin, P. (2008) Origin of the 1915 Lassen Peak eruption by magma mixing: Evidence for formation of chemically distinct plagioclase populations from crystal size distributions and in situ chemical data. Journal of Petrology 49, 1755–1780.

Sparks, R.S.J., Sigurdsson H. & Wilson, L. (1977) Magma mixing: a mechanism for triggering acid explosive eruptions. Nature 267, 315-318.

Sun S.-S. & McDonough W.F. (1989) Chemical and isotopic systematics of oceanic basalts: implications for mantle composition and processes. Magmatism in the Ocean Basins, Saunders AD & Norry MJ (eds). Geological Society Special Publication 42, 313-345.

Tsuchiyama, A. (1985) Dissolution kinetics of plagioclase in the melt system diopside-albite-anorthite, and origin of dusty plagioclase in andesites. Contributions to Mineralogy and Petrology 89, l-16.

Witter, M.R., Geirsson, H., LaFemina, P.C., Roman, D.C., Rodgers, M., Muñoz, A., Tenorio, V., Chavarria, D., Feineman, M.D., Furman, T. & Longley, A. (2011) May 2011 eruption of Telica volcano, Nicaragua: Multidisciplinary observations, Abstract V53E-2670 presented at 2011 Fall Meeting, AGU, San Francisco, Calif., 5-9 Dec.

Figure Captions

Figure 1: a) Geographical map of Nicaragua illustrating the proximity of Telica to the populated cities of Leòn and Managua. b) Topographic map of Telica showing sample locations. The crosshair indicates the active crater.

Figure 2: Microfiche scan of thin section MT11-1 showing rectangular, sieve-textured and zoned plagioclase phenocrysts. S-plg denotes two heavily sieved plagioclase feldspar phenocrysts.

Figure 3: Total alkalis-silica plot for Telica lavas. CR-P open circles denote Telica lava and bomb samples from Carr and Rose (1987) and Patino et al., (2000). Filled diamonds denote samples from this study. The gray shaded field represents Central American lavas from Costa Rica, Guatemala, El Salvador and Honduras (Carr and Rose, 1987; Patino, 2000).

Figure 4: a) Rare earth element abundances of the most mafic (MT11-1, MT11-2, MT11-12) and felsic samples (MT11-6, MT11-7) normalized to chondritic values of Sun and McDonough (1989). Light gray and dark gray shaded fields represent Telica lavas from Carr and Rose (1987) and Patino et al. (2000) and this study, respectively. b) Primitive mantle normalized incompatible trace element diagram (Sun & McDonough, 1989) illustrating the saw tooth pattern typical of Telica lavas (shaded fields from Carr and Rose, 1987; Carr et al., 2007; Patino et al., 2000).

Figure 5: Ba/Th versus U/La plot for Telica lavas. CR-P open circles denote Telica lava and bomb samples from Carr and Rose (1987) and Patino et al., (2000), few with associated eruption ages. Filled diamonds denote samples from this study. The parabolic curve represents variable mixes of melt and subducted hemipelagic sediments. Higher U/La and lower Ba/Th signifies larger hemipelagic sediment contributions.

Figure 6: Plagioclase crystal size distribution curves for 14 Telica lava samples, showing ln(population density) versus phenocryst length (mm). Linear segments define two distinct crystal populations: S1 <1.5 mm and S2 >1.5 mm. MT11-12 (dashed line) has the greatest upward concavity; MT11-RB (dotted line) is the most linear CSD curve.

Figure 7: Back scattered electron images of typical plagioclase feldspar phenocrysts set in a plagioclase and Fe-Ti oxide-dominated matrix. Plagioclase 4 and 5 are both from MT11-12, the most mafic sample collected during this study. The core of plagioclase 4 is clearly sieved and has a composition of An75. The core of plagioclase 5 is not sieved and has a composition of An89.

Figure 8: Plot illustrating the core and rim anorthite contents of plagioclase phenocrysts from both size fractions (S1 and S2) for a mafic sample (MT11-12) and a more evolved sample (MT11-7). The more magnesian sample, MT11-12, generally has lower rim and core anorthite contents. The S1 populations are noticeably different between the two samples.

Tables

This is a preprint, the final version is subject to change, of the American Mineralogist (MSA)
Cite as Authors (Year) Title. American Mineralogist, in press.
(DOI will not work until issue is live.) DOI: http://dx.doi.org/10.2138/am-2016-5379

Sample	MT11-1	MT11-2	MT11-3	MT11-4	MT11-5	MT11-6	MT11-7	MT11-8	MT11-9	MT11-10	MT11-11	MT11-12	MT11-CW	MT11-RB
SiO_2**	51.16	51.47	51.76	52.13	51.25	53.65	53.62	54.19	51.88	50.27	49.81	51.18	50.80	48.48
Al_2O_3	16.79	17.09	17.21	17.60	17.38	17.96	18.34	16.96	17.58	18.16	18.41	17.03	18.25	19.37
TiO_2	1.42	1.48	0.99	0.80	0.79	0.74	0.75	1.09	1.17	0.83	0.77	1.47	0.69	0.82
Fe_2O_3*	10.75	11.10	10.50	10.68	10.44	9.97	10.06	9.84	10.57	10.58	10.80	11.04	10.52	11.27
MgO	5.95	6.02	5.36	4.61	4.47	4.06	4.03	4.98	5.32	5.21	5.42	6.14	5.03	4.51
MnO**	0.16	0.16	0.17	0.19	0.18	0.17	0.17	0.16	0.17	0.17	0.18	0.16	0.18	0.19
CaO	9.82	10.10	10.62	9.86	9.66	9.49	9.62	9.61	10.08	10.65	11.04	10.02	10.25	11.06
Na_2O	2.79	2.79	2.64	2.79	2.77	2.57	2.61	2.94	2.72	2.49	2.39	2.82	2.41	2.33
K_2O	1.18	1.04	1.23	1.48	1.81	1.91	2.15	1.22	1.44	1.19	1.08	1.06	1.44	0.36
P_2O_5	0.17	0.21	0.17	0.15	0.14	0.20	0.19	0.18	0.19	0.19	0.14	0.20	0.13	0.14
total	100.19	101.47	100.65	100.29	98.89	100.72	101.56	101.16	101.11	99.73	100.05	101.13	99.69	98.54
LOI	0.6	0.4	0.0	-0.2	-0.3	0.7	0.6	0.1	0.2	0.4	0.0	-0.4	0.6	1.2
Ni	70.7	68.7	22.5	10.6	11.3	7.9	8.5	40.7	40.5	19.5	18.7	73.3	13.8	10.9
Rb	17.4	16.6	22.4	25.5	26.5	29.8	29.6	24.5	23.7	20.6	20.1	17.6	16.4	4.9
Sr	425.2	402.2	480.2	474.4	491.2	435.4	463.2	454.1	443.9	493.7	513.3	436.4	438.9	528.2
Ba	425.9	412.6	572.9	702.8	747.9	802.3	817.5	611.1	585.0	580.6	570.1	422.1	689.9	486.2
La	5.91	5.77	6.28	5.83	6.51	6.78	6.53	6.80	6.55	5.79	5.19	5.97	5.11	4.73
Ce	14.46	13.88	14.88	14.14	15.26	15.57	15.22	16.14	15.34	13.41	12.35	14.37	12.05	10.83
Pr	2.30	2.24	2.38	2.25	2.45	2.50	2.46	2.65	2.48	2.17	2.08	2.34	1.89	1.82
Nd	11.48	10.92	11.19	10.77	11.90	11.30	11.20	12.40	12.06	10.47	9.67	11.51	9.34	8.84
Sm	3.45	3.31	3.23	2.89	3.13	3.10	2.94	3.44	3.38	2.89	2.70	3.51	2.59	2.55
Eu	1.23	1.21	1.11	0.93	1.06	0.96	0.96	1.19	1.14	0.99	0.93	1.26	0.89	0.95
Tb	0.69	0.66	0.61	0.57	0.62	0.61	0.58	0.69	0.63	0.56	0.54	0.68	0.55	0.52
Gd	4.10	3.93	3.69	3.50	3.78	3.57	3.54	3.98	3.87	3.35	3.24	4.20	3.08	2.96
Dy	4.11	3.91	3.83	3.72	3.97	3.85	3.78	4.03	3.99	3.62	3.44	4.12	3.46	3.29
Ho	0.79	0.76	0.76	0.74	0.81	0.81	0.80	0.79	0.78	0.70	0.70	0.81	0.72	0.68
Er	2.05	2.02	2.07	2.17	2.21	2.32	2.19	2.21	2.10	1.93	1.86	2.03	1.95	1.91
Yb	1.86	1.78	1.96	2.16	2.22	2.17	2.27	2.10	2.08	1.91	1.82	1.81	2.04	1.84
Lu	0.29	0.28	0.30	0.33	0.34	0.37	0.37	0.35	0.31	0.30	0.30	0.28	0.31	0.29
Li	6.05	5.49	6.72	8.09	8.54	8.18	7.68	6.64	6.02	6.56	6.26	5.89	7.07	5.51
Be	0.65	0.58	0.66	0.46	0.49	0.59	0.64	0.73	0.69	0.43	0.49	0.74	0.44	0.44
Sc	27.54	26.58	31.28	30.01	30.62	28.17	28.15	27.00	25.39	30.46	32.92	28.56	30.65	29.66
V	236.38	236.39	297.46	319.45	300.64	269.00	269.65	256.40	244.59	309.52	347.49	251.70	296.63	316.40
Cr	119.22	105.64	36.64	12.80	11.98	10.85	10.81	69.01	62.33	29.19	18.28	124.80	6.45	7.57
Co	45.79	41.77	43.05	41.01	51.01	37.72	37.67	41.98	65.37	40.73	56.04	70.56	46.27	35.07
Cu	129.69	125.98	153.68	174.09	182.00	128.92	132.95	144.09	142.60	161.07	165.19	133.69	176.60	174.54
Zn	91.38	87.35	81.75	104.38	84.32	75.83	78.82	84.07	81.37	78.74	85.91	104.33	77.66	81.08
Y	21.35	20.43	20.79	21.31	22.13	22.88	22.60	21.40	21.29	19.37	19.25	21.85	19.51	18.82
Zr	98.38	95.57	88.78	79.80	85.17	93.81	89.59	99.87	100.12	70.67	62.50	102.68	68.73	48.77
Nb	10.40	10.21	6.08	1.88	2.12	1.99	1.74	7.54	7.33	2.78	1.61	11.01	1.41	1.00
Mo	0.87	0.81	0.83	0.77	0.76	0.93	0.90	0.92	0.96	0.67	0.62	0.85	0.62	0.40
Cs	0.64	0.60	0.82	1.00	1.11	1.17	1.18	0.89	0.99	0.85	0.83	0.60	0.43	0.18
Hf	2.73	2.69	2.47	2.15	2.46	2.61	2.53	2.82	2.81	2.00	1.81	2.83	2.04	1.44
Ta	0.70	0.71	0.41	0.17	0.19	0.16	0.13	0.51	0.48	0.20	0.13	0.70	0.13	0.08
Pb	1.98	1.72	2.64	3.22	3.42	3.66	3.58	2.76	2.66	2.71	2.60	2.00	2.97	2.25
Th	0.82	0.81	1.04	1.13	1.25	1.41	1.43	1.21	1.17	0.96	0.88	0.85	0.98	0.67
U	0.65	0.62	0.90	1.06	1.15	1.30	1.26	1.01	0.99	0.89	0.79	0.69	0.90	0.49

Table 1: Major (wt. %) and select trace (ppm) elemental geochemical data for Telica samples from this study. LOI values are provided from the raw data as an analog for sample freshness. $Fe_2O_3^{*}$ denotes total iron (Fe^{2+} and Fe^{3+} species). SiO_2^{**} and MnO^{**} denote that samples were analyzed twice and averaged for each.

Sample	Area measured (mm^2)	Number of crystals measured	Intercept	S1 slope	S1 Residence Time (yr)	S2 slope	S2 Residence Time (yr)	□ Slope (S2-S1)
MT11-12	722	479	2.818	-5.2	61	-1.0	317	4.2
MT11-1	722	311	2.323	-5.3	60	-4.1	77	1.2
MT11-2	450	329	2.886	-5.1	62	-2.2	144	2.9
MT11-11	400	515	3.551	-5.4	59	-1.6	198	3.8
MT11-3	722	425	3.054	-4.9	65	-2.2	144	2.7
MT11-9	400	506	3.155	-5.3	60	-2.0	159	3.3
MT11-10	400	445	3.145	-5.1	62	-2.8	113	2.3
MT11-CW	700	410	2.780	-5.0	63	-1.0	317	4.0
MT11-8	360	511	3.113	-5.1	62	-1.3	244	3.8
MT11-4	722	435	2.741	-5.0	63	-2.3	138	2.7
MT11-RB	722	450	2.568	-4.8	66	-4.2	75	0.6
MT11-5	722	416	2.271	-4.5	70	-2.1	151	2.4
MT11-6	722	494	2.440	-5.2	61	-2.8	113	2.4
MT11-7	360	459	2.984	-5.0	63	-1.6	198	3.4
			Avg. = 2.84	Avg. = -5.1	Avg. ~63 yrs	Avg. = -2.2	Avg. ~171 yrs	

Table 2: CSD parameters and slope measurements for both plagioclase populations for each sample. Samples are organized in the table from most mafic to most felsic. All CSD curves were calculated using a 1.0:3.4:4.0 aspect ratio and maximum length phenocryst measurements. Average crystal residence times were calculated using the measured slopes and an assumed growth rate of 10^{-10}mm/s (Cashman and March, 1988; Cashman, 1988). Delta slope is synonymous with the degree of upward concavity.

Sample	MT11-12																			
Size Pop.	S1										S2									
ID #	7		8		9		10		11		1		2		3		4		5	
	Core	Rim	Core	Rim	Core	Rim	Core	Rim	Core	Rim	Core	Rim	Core	Rim	Core	Rim	Core	Rim	Core	Rim
SiO2	50.5	54.1	49.9	53.0	50.4	54.4	48.4	53.2	48.8	53.9	45.3	50.0	48.2	53.0	48.5	50.7	49.0	53.1	45.8	53.5
Al2O3	30.5	27.3	31.1	28.8	30.9	28.1	31.9	28.4	31.8	28.1	34.1	31.1	32.2	28.7	32.2	30.4	31.4	28.8	34.0	28.5
FeO*	0.9	1.2	0.8	0.9	0.8	1.1	0.7	1.1	0.7	1.1	0.5	0.5	0.7	0.9	0.7	0.8	0.7	0.8	0.7	0.9
MgO	0.2	0.4	0.1	0.2	0.2	0.2	0.1	0.2	0.1	0.2	0.0	0.1	0.1	0.2	0.1	0.2	0.1	0.2	0.1	0.2
CaO	14.6	11.8	15.2	12.6	15.0	11.8	16.1	12.4	16.1	11.8	18.3	14.7	16.3	12.5	16.1	14.4	15.4	12.6	18.2	12.3
Na2O	3.2	4.7	2.8	4.1	3.0	4.6	2.2	4.1	2.5	4.4	1.1	3.1	2.3	4.2	2.3	3.2	2.7	4.2	1.2	4.4
K2O	0.1	0.4	0.1	0.3	0.1	0.3	0.1	0.3	0.1	0.4	0.0	0.2	0.1	0.2	0.1	0.1	0.1	0.3	0.0	0.3
Total	100.0	99.9	100.0	99.9	100.3	100.4	99.5	99.7	100.1	99.8	99.3	99.6	99.9	99.7	100.1	99.8	99.3	100.0	100.0	100.0
An	71	57	74	62	73	56	79	61	78	58	90	72	79	61	79	71	75	61	89	60

Sample	MT11-7																			
Size Pop.	S1										S2									
ID #	18		19		20		21		22		12		13		14		15		16	
	Core	Rim	Core	Rim	Core	Rim	Core	Rim	Core	Rim	Core	Rim	Core	Rim	Core	Rim	Core	Rim	Core	Rim
SiO2	46.5	48.9	45.7	53.2	48.1	53.1	44.8	50.3	45.1	48.7	46.6	49.8	47.1	51.1	47.4	45.8	45.5	49.4	47.4	49.1
Al2O3	33.4	31.2	34.2	28.7	32.5	28.6	34.5	30.5	34.5	31.5	33.3	31.0	33.3	29.8	32.8	34.1	34.1	31.3	33.2	31.1
FeO*	0.8	1.0	0.8	1.3	0.8	1.1	0.8	1.0	0.8	0.8	0.8	1.0	0.8	1.1	0.8	0.9	0.8	0.9	0.7	0.9
MgO	0.1	0.2	0.1	0.2	0.1	0.1	0.0	0.1	0.1	0.1	0.1	0.2	0.1	0.2	0.1	0.1	0.1	0.2	0.1	0.1
CaO	17.8	15.7	18.6	12.7	16.5	12.5	18.9	14.7	18.7	15.8	17.5	15.5	17.6	14.1	16.8	18.4	18.4	15.4	17.1	15.5
Na2O	1.5	2.5	1.0	4.2	2.1	4.1	0.8	3.0	0.9	2.3	1.5	2.8	1.5	3.4	1.8	1.1	1.1	2.7	2.0	2.6
K2O	0.0	0.1	-0.3	0.4	0.1	0.3	0.1	0.2	0.0	0.1	0.1	0.2	0.0	0.3	0.1	0.0	0.0	0.1	0.1	0.1
Total	100.2	99.5	100.1	100.5	100.1	99.9	99.9	99.8	100.1	99.4	99.8	100.5	100.5	99.8	99.8	100.4	100.0	99.9	100.5	99.5
An	87	77	91	61	81	62	93	72	92	64	86	75	86	67	83	90	90	75	82	76

Table 3: Electron microprobe analysis results for major oxides from representative plagioclase feldspar phenocrysts from samples MT11-12 and MT11-7. S1 size population represents phenocrysts <1.5mm and S2 >1.5mm. Anorthite contents were calculated for core and rim measurements of the phenocrysts.

This is a preprint, the final version is subject to change, of the American Mineralogist (MSA)
Cite as Authors (Year) Title. American Mineralogist, in press.
(DOI will not work until issue is live.) DOI: http://dx.doi.org/10.2138/am-2016-5379

Figure 1

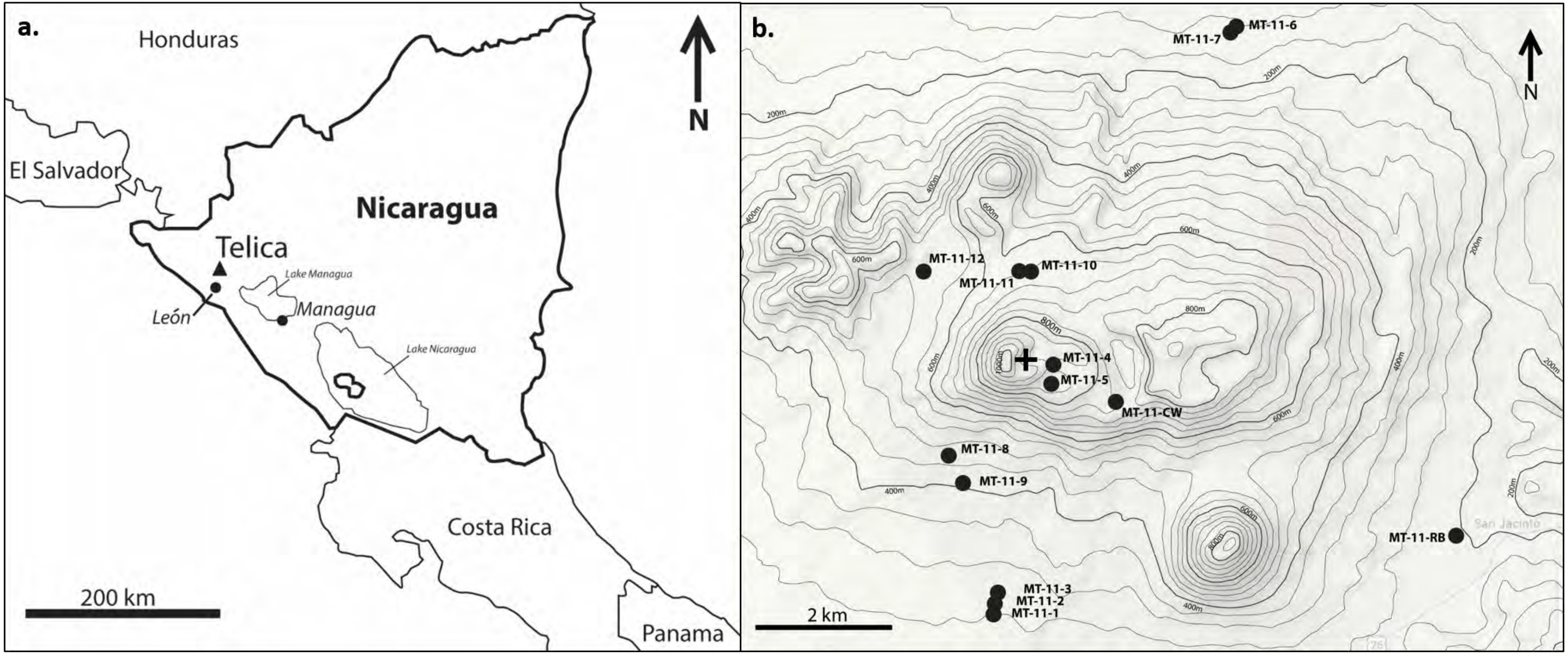

This is a preprint, the final version is subject to change, of the American Mineralogist (MSA)
Cite as Authors (Year) Title. American Mineralogist, in press.
(DOI will not work until issue is live.) DOI: http://dx.doi.org/10.2138/am-2016-5379

Figure 2

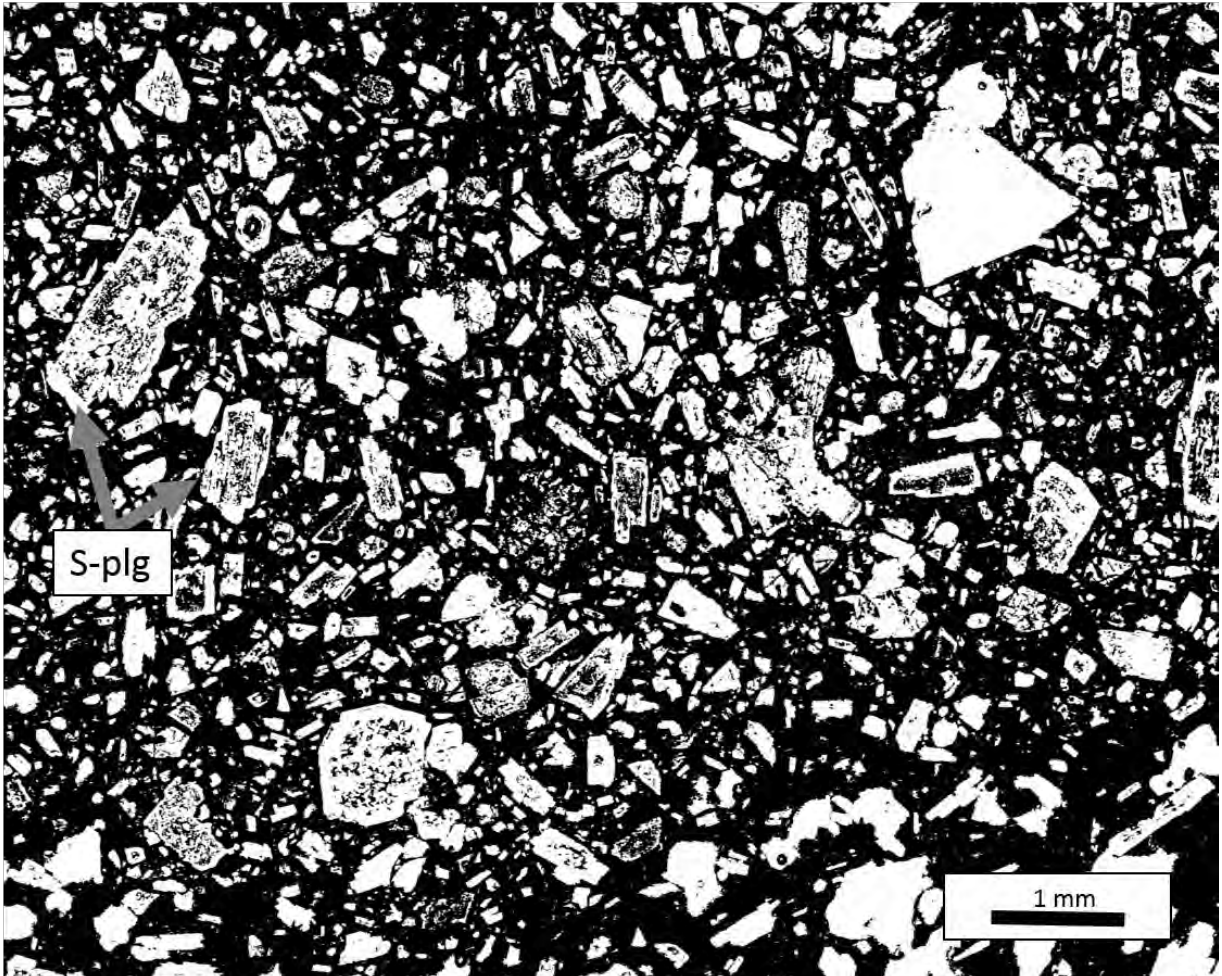

(DOI will not work until issue is live.) DOI: http://dx.doi.org/10.2138/am-2016-5379

Figure 3

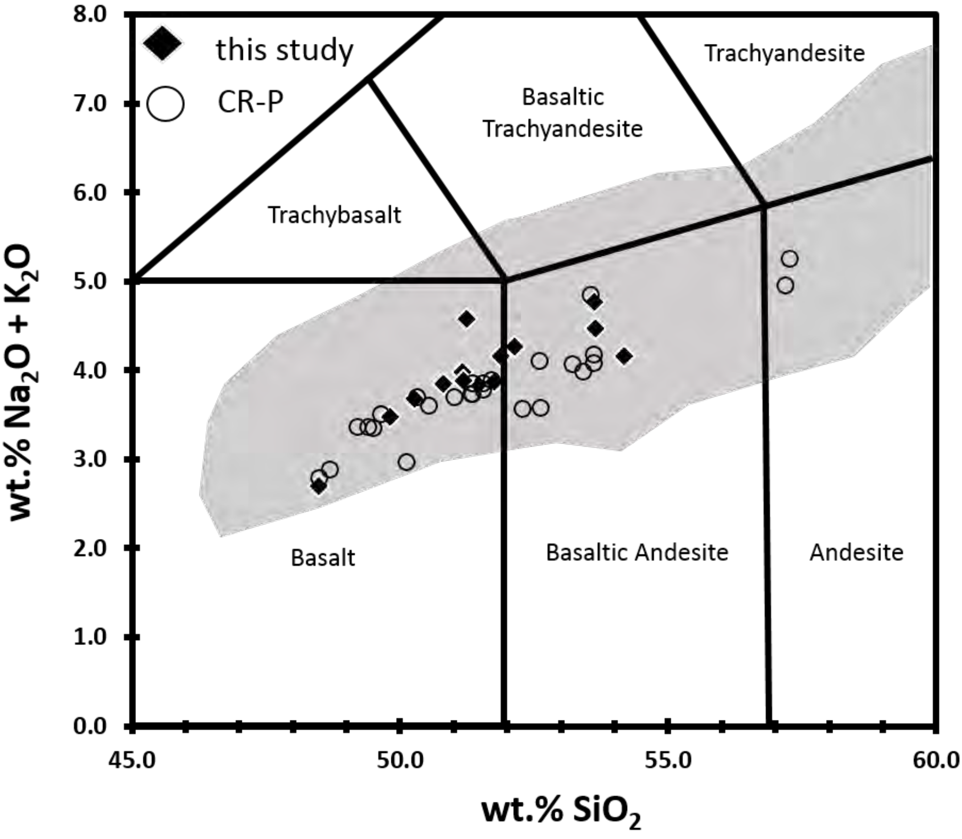

This is a preprint, the final version is subject to change, of the American Mineralogist (MSA)
Cite as Authors (Year) Title. American Mineralogist, in press.
(DOI will not work until issue is live.) DOI: http://dx.doi.org/10.2138/am-2016-5379

Figure 4

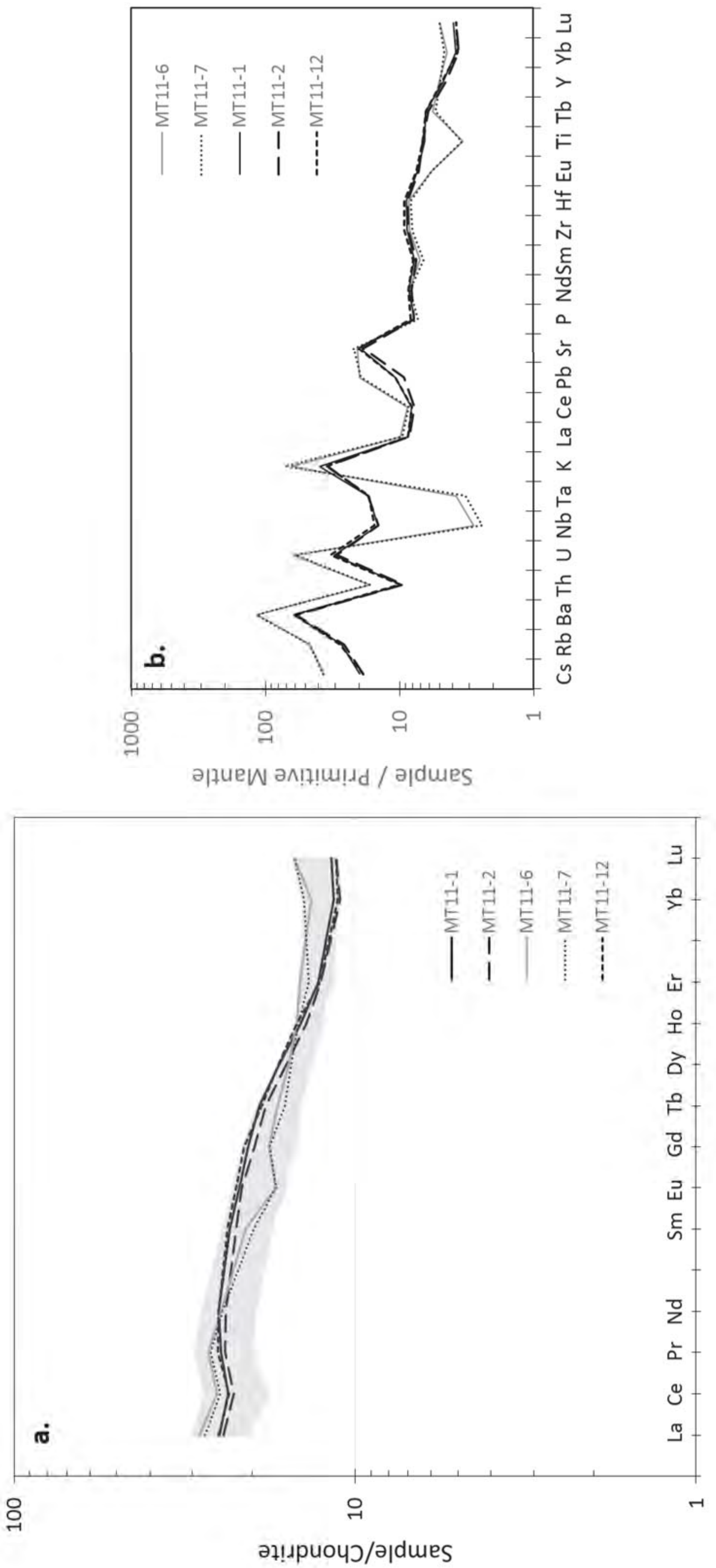

Figure 5

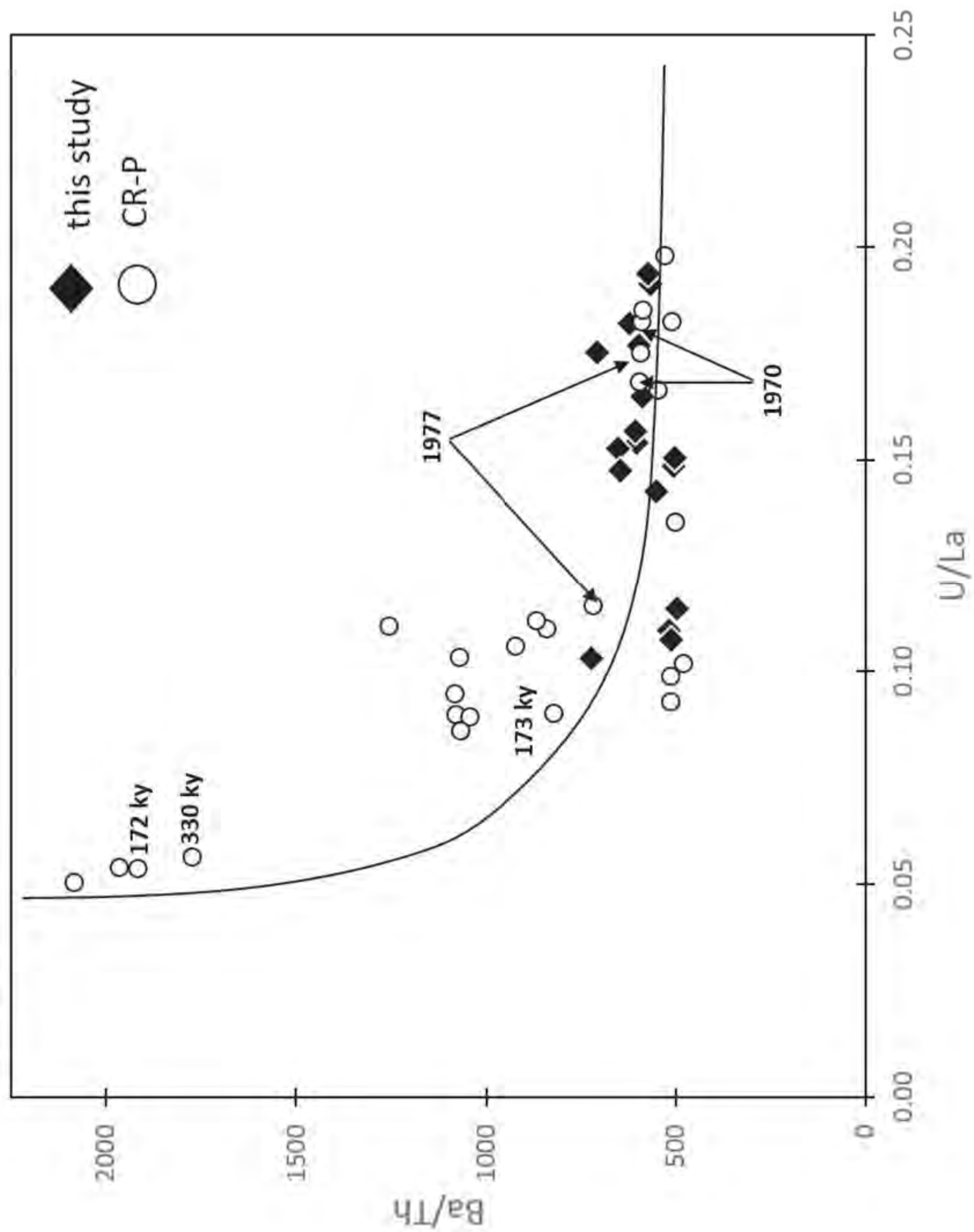
this study
CR-P
1977
1970
172 ky
330 ky
173 ky
U/La
Ba/Th
0.00
0.05
0.10
0.15
0.20
0.25
0
500
1000
1500
2000

Figure 6

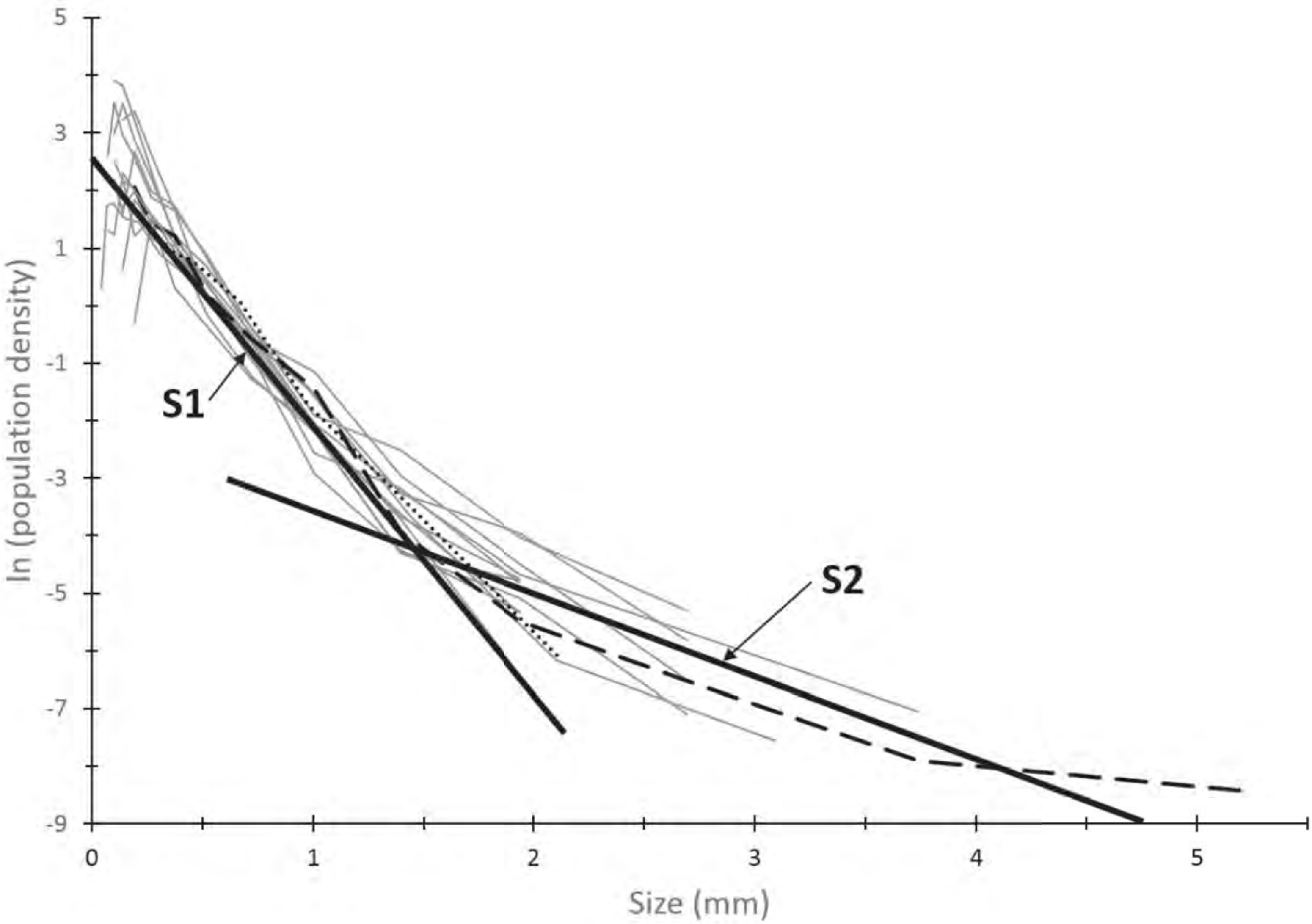

This is a preprint, the final version is subject to change, of the American Mineralogist (MSA)
Cite as Authors (Year) Title. American Mineralogist, in press.
(DOI will not work until issue is live.) DOI: http://dx.doi.org/10.2138/am-2016-5379

Figure 7

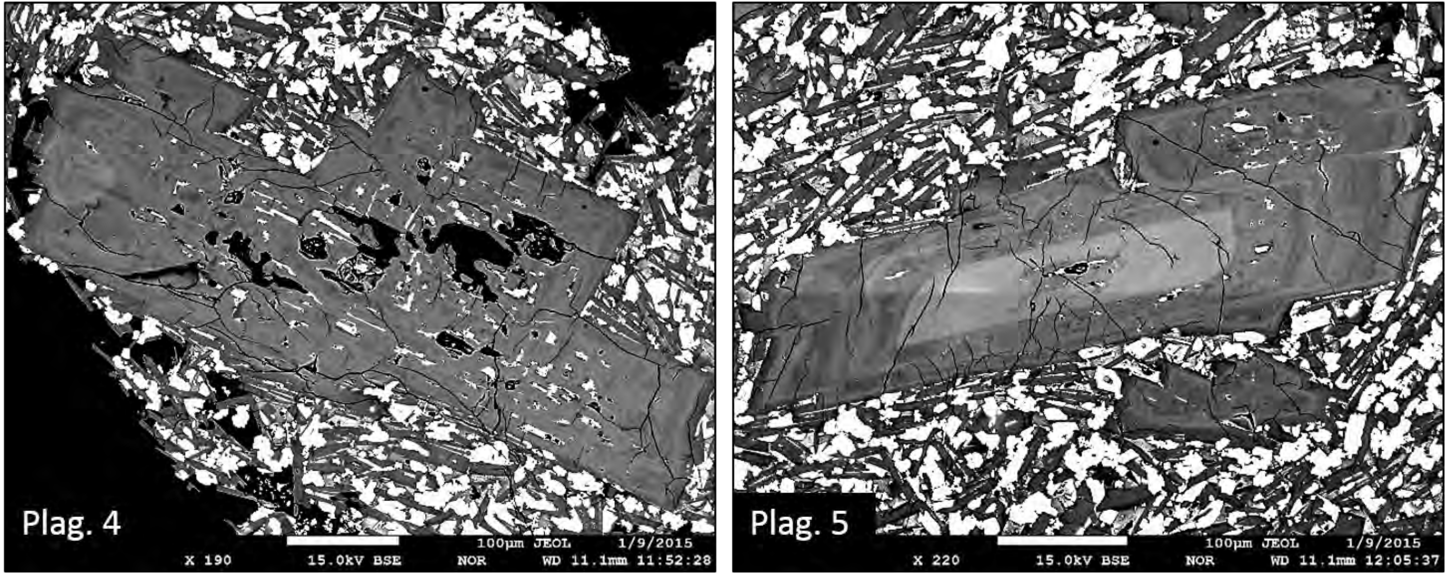

Figure 8

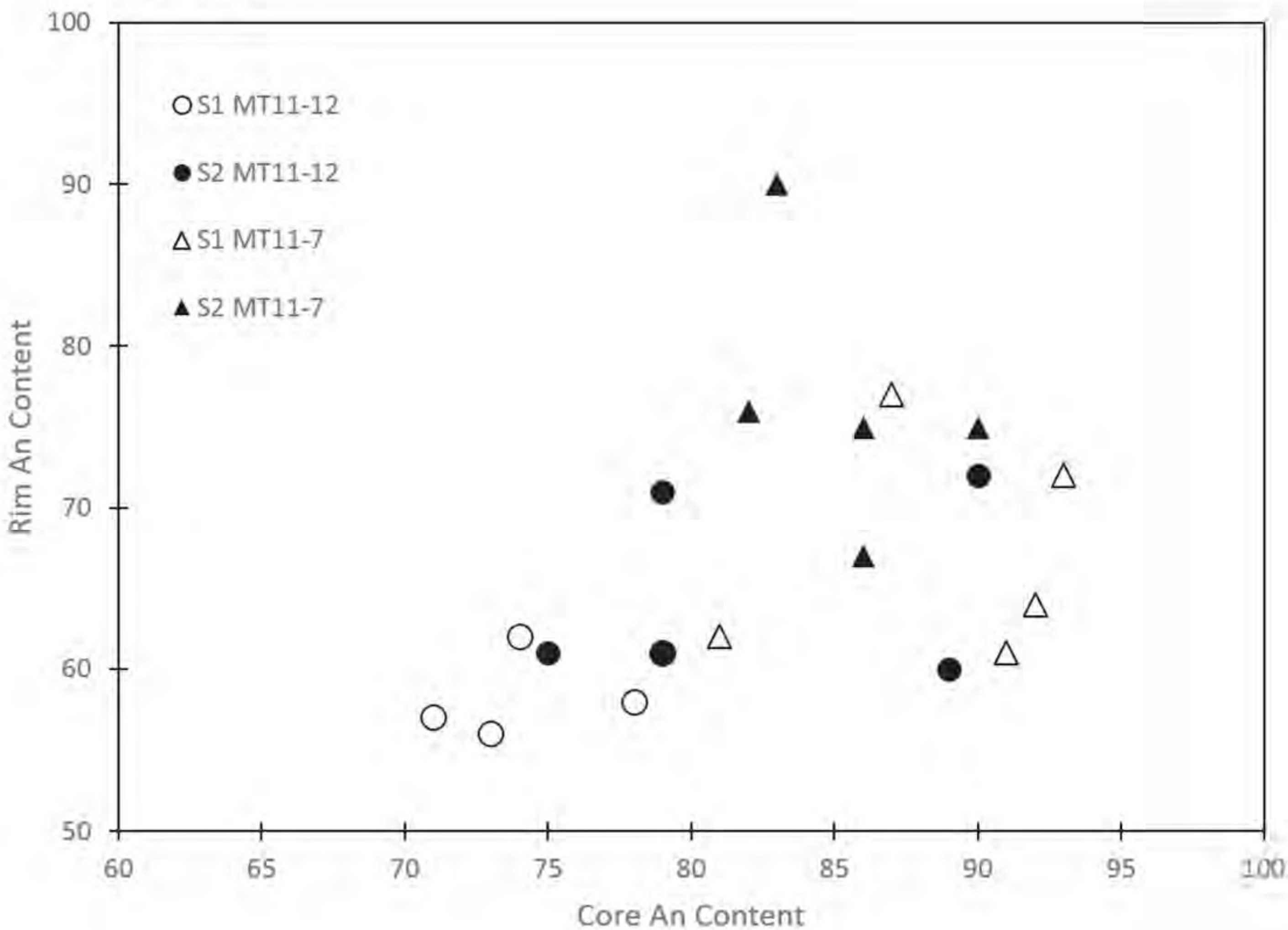
S1 MT11-12
S2 MT11-12
S1 MT11-7
S2 MT11-7
Rim An Content
Core An Content
100
90
80
70
60
50
60
65
70
75
80
85
90
95
100